Modelling stream flow and quantifying blue water using a modified STREAM model for a heterogeneous, highly utilized and data scarce river basin in Africa.

J. K. Kiptala[1,2], M.L. Mul[1,3], Y. Mohamed[1,4,5], and P. van der Zaag[1,4]

[1]UNESCO-IHE, Institute for Water Education, P.O. Box 3015, 2601 DA Delft, The Netherlands

[2]Jomo Kenyatta University of Agri. and Technology, P.O Box 62000, 00200 Nairobi, Kenya

[3]International Water Management Institute, PMB CT 112, Cantonments, Accra, Ghana

[4]Delft University of Technology, P.O Box 5048, 2600 GA Delft, The Netherlands

[5]Hydraulic Research Center, P.O Box 318, Wad Medani, Sudan

Correspondence to: J. K. Kiptala (j.kiptala@unesco-ihe.org, kiptalajeremy@yahoo.com)

Abstract

Integrated water resources management is a combination of managing blue and green water resources. Often the main focus is on the blue water resources, as information on spatially distributed evaporative water use is not readily available as is the link to river flows. Physically based spatially distributed models are often used to generate this kind of information. These models require enormous amounts of data, which can result in equifinality, making them less suitable for scenario analyses. Furthermore, hydrological models often focus on natural processes and fail to account for anthropogenic influences. This study presents a spatially distributed hydrological model that has been developed for a heterogeneous, highly utilized and data scarce river basin in Eastern Africa. Using an innovative approach, remote sensing derived evapotranspiration and soil moisture variables for three years were incorporated as input data in the Spatial Tools for River basin Environmental Analysis and Management (STREAM) model. To cater for the extensive irrigation water application, an additional blue water component (Q_b) was incorporated in the STREAM model to quantify irrigation water use. To enhance model parameter identification and calibration, three hydrological landscapes (wetlands, hill-slope and snowmelt) were identified using field data. The model was calibrated against discharge data from five gauging stations and showed a good performance especially in the simulation of low flows where the Nash-Sutcliffe Efficiency of the natural logarithm (E_{ns_ln}) of discharge were greater

than 0.6 in both calibration and validation periods. At the outlet, the E_{ns_ln} coefficient was even higher (0.90). During low flows, Q_b consumed nearly 50% of the river flow in the basin. Q_b model result for irrigation was comparable to the field based net irrigation estimates with less than 20% difference. These results show the great potential of developing spatially distributed models that can account for supplementary water use. Such information is important for water resources planning and management in heavily utilized catchment areas. Model flexibility offers the opportunity for continuous model improvement when more data become available.

1   Introduction

Hydrological models are indispensable for water resource planning and management at catchment scale as these can provide detailed information on, for example, impacts of different scenarios and trade-off analyses. Society's demand for more accountability in the management of externalities between upstream and the downstream water users has also intensified the need for more predictive and accurate models. However, complexity of hydrological processes and high levels of heterogeneity present considerable challenges in model development. Such challenges have been exacerbated over time by land use changes that have influenced the rainfall partitioning into *green* (soil moisture) and *blue* (runoff) water resources. In spite of these challenges, it is still desirable to develop a distributed hydrological model that can simulate the dominant hydrological processes and take into account the various water uses. In large catchments with high heterogeneity, key variables such as water storage (in unsaturated and saturated zones) and evaporation (including transpiration) are difficult to obtain directly from point measurements. This becomes even more difficult for ungauged or poorly gauged river basins.

In most cases those variables are derived from models using (limited) river discharge data which increases equifinality problems (Savenije, 2001; Uhlenbrook et al., 2004; McDonnell et al., 2007; Immerzeel and Droogers, 2008). On the other hand, grid based distributed models at fine spatial scales do not explicitly account for additional *blue water* use (Q_b), i.e. transpiration from supplementary irrigation or withdrawals from open water evaporation. In fact in tropical arid regions, Q_b can be a large percentage of the river discharge during low flow. Calibrating models using modified stream flow data may lead to incorrect parameterization, and may lead to high

2

predictive uncertainty in the hydrological model outputs especially when dealing with scenarios for water use planning.

To overcome these challenges, many researchers have opted for simple, lumped and or parsimonious models with a limited number of model parameters. The models are simplified by bounding and aggregation of some functionality in the complex system (Winsemius et al., 2008). In doing so, models may become too simplified to represent hydrological processes in a catchment (Savenije, 2010). Therefore, Savenije (2010) proposes a conceptual model mainly based on topographic characteristic to represent the dominant hydrological processes. The model maintains the observable landscape characteristics and requires a limited number of parameters. Other researchers have used secondary data, e.g. from remote sensing to calibrate or infer model parameters as much as possible (Winsemius et al., 2008; Immerzeel and Droogers, 2008; Campo et al., 2006). This has been possible in the recent past because of the availability of satellite images with finer spatial resolutions. Advancement in remote sensing algorithms has also resulted in wider range spatial data of reasonably good accuracies. Such spatial data include actual evapotranspiration (ET_a) derived from remote sensing data, e.g. TSEB (Norman et al., 1995), SEBAL (Bastiaanssen et al., 1998a; 1998b), S-SEBI (Roerink et al., 2000), SEBS (Su, 2002) and METRIC (Allen et al., 2007). Spatial data on soil moisture can also be derived from satellite images, e.g. from ERS-1 Synthetic Aperture Radar (SAR) combined with the TOPMODEL topographic index (Scipal et al., 2005) or from Advance Very High Resolution Radiometer (AVHRR) combined with the SEBAL model (Mohamed et al., 2004). It is also evident that distributed models perform well with finer resolution data as demonstrated by Shrestha et al. (2007). Using different resolution data (grid precipitation and grid ET_a) and a concept of IC ratio (Input grid data area to Catchment area) they found that a ratio higher than 10 produces a better performance in the Huaihe River Basin and its sub-basin of Wangjiaba and Suiping in China (Shrestha et al., 2007).

Furthermore, remotely sensed data at finer resolutions offer great potential for incorporating blue water, in the form of (supplementary) water use (Q_b) in model conceptualization. This opportunity arises from the fact that remotely sensed ET_a based on energy balance provides total evapotranspiration that already accounts for Q_b. For instance, Romaguera et al. (2012) used the difference between Meteosat Second Generation (MSG) satellites data (total ET_a) and Global Land Data Assimilation System (GLDAS) which does not account for Q_b, to quantify blue water

use for croplands in Europe with a reasonable accuracy. However, the spatial scales of such datasets (GLDAS (1 km) and MSG (3 km)) limit the application. Nevertheless, the latter recommended such application to recently available data of wider spatial and temporal coverage, e.g. data derived from Moderate-resolution Imaging Spectroradiometer (MODIS) 250-m, 500-m.

5   However, the literature shows limited applications of utilizing grid data for distributed hydrological models in poorly gauged catchments. Winsemius et al. (2006) showed that the soil moisture variations from the Gravity Recovery And Climate Experiment (GRACE) could provide useful information to infer and constrain hydrological model parameters in the Zambezi river basin. Campo et al. (2006) using an algorithm developed by Nelder and Mead (1965), used

10   remotely sensing soil moisture information to calibrate a distributed hydrological model in the Arno basin, Italy. Immerzeel and Droogers (2008) used remotely sensed ET_a derived from SEBAL in the calibration of a Soil and Water Assessment Tool (SWAT) model of the Krishna basin in southern India in which the model performance (r^2) increased from 0.40 to 0.81. Recently, Cheema et al. (2014) has used satellite derived rainfall to parameterize the SWAT

15   model while ET_a from ETLook was used to calibrate the model to determine the contribution of groundwater use to the total blue water use in the Indus Basin.

The factors that may have limited the application of remote sensing (RS) data on hydrological modelling include: a) Limited flexibility of hydrological models to utilize spatially distributed data. This is normally the case where the user has no control over the model source code. The

20   user is therefore limited to optimizing model performance using secondary data. b) Limited availability of RS data at the appropriate spatial and temporal scales to capture dominant hydrological processes in a catchment. c) The lack of technical skills by most hydrologists and water resource specialists on how to transform RS data into hydro-meteorological data (Schultz, 1993). The opportunities and challenges for the wider application of remote sensing for

25   hydrological modelling are discussed by De Troch et al. (1996) and Schultz (1993).

This paper presents a novel method of using ET_a and soil moisture data derived from satellite images as input in a distributed hydrological model. The Upper Pangani River Basin in Eastern Africa has been used as a case study. This river basin has heavily managed landscapes dominated by small and large scale irrigated agriculture. The secondary data used in this study have been

30   generated using MODIS satellite information and the SEBAL model on 250-m and 8-day resolutions for the period 2008-2010 (Kiptala et al., 2013b). Here the STREAM model has been

modified to incorporate blue water use. The model parameters have also been confined further by the topographic characteristics and groundwater observations using the hydrological conceptualization developed by Savenije (2010).

2 Study area

The Upper Pangani River Basin (13,400 km^2) covers approximately 30% of the total area of the Pangani River Basin and is located in Eastern Africa (Fig. 1). It is the main headwaters of the basin and derives its water sources from the Mt. Kilimanjaro (5,880 metres above sea level (m.a.s.l)) and Mt. Meru (4,565 m.a.s.l) catchments. The flows to the lower basin are regulated by a large dam (storage capacity 1.1×10^9 m^3), the Nyumba ya Mungu (NyM) reservoir. The Lower Pangani River Basin has three operational hydro-electric power (HEP) stations: NyM HEP, Hale HEP and the New Pangani Falls HEP station. These provide up to 91.5 MW or 17% of Tanzania's electricity.

The catchment has a highly varied climate mainly influenced by topography. The high altitude slopes around the mountain ranges, have an Afro-Alpine climate and receive nearly 2,500 mm y^{-1} of rainfall. The lower parts have a sub-humid to semi-arid climate and the rainfall varies between 300 to 800 mm y^{-1}. The rainfall has a bimodal pattern where long rains are experienced in the months of March to May (*Masika* season) and the short rains in the months of November and December (*Vuli* season). It is during these two seasons when most crops are grown. Rainfed and supplementary irrigated croplands are the dominant agricultural systems. However, grasslands and shrublands are also dominant land use types (see section 3.2) (Kiptala et al., 2013a).

<INSERT FIGURE 1>

3 Materials and methods

3.1 Datasets

3.1.1 Hydro-meteorological data

Daily rainfall data for 93 stations located in or near the Upper Pangani River Basin were obtained from the Tanzania Meteorological Agency and the Kenya Meteorological Department. The data was screened and checked for stationarity (Dahmen and Hall, 1990). Of the original group, 43 stations proved useful after data validation for the period 2008 - 2010. Unfortunately, there were no rainfall stations at elevations higher than 2,000 m a.s.l. where the highest rainfall actually occurs. Spatially distributed rainfall can also be provided by satellite sensors to augment

rainfall data from the ground stations (Huffman et al., 2001). Such satellites sensors include the Tropical Rainfall Measuring Mission (TRMM). Famine Early Warning System (FEWS) product also provides remotely sensed rainfall data in Africa. The satellite based rainfall has uncertainties that can be corrected using limited ground rainfall measurements (Hong et al., 2006; Cheema and Bastiaanssen, 2012). Since there were no rainfall stations at the mountainous areas, the satellite based rainfall could not be validated (Haque, 2009).

According to PWBO / IUCN (2006), the maximum long term mean annual precipitation (MAP) at the Pangani River Basin is estimated at 3,453 mm yr^{-1} at elevation 2,453 m.a.s.l. The estimates were based on a rain gauge station that is no longer operational. Therefore, a linear extrapolation method based on the concept of double mass analysis (Wilson, 1983) was used to derive the seasonal rainfall up to the mountain peaks. Double mass analysis assumes relatively consistent correlation between time series of rainfall data at nearby stations with similar hydrological conditions (Chang and Lee, 1974). In the analysis, the seasonal precipitation at the mountain peak (Y) is assumed to have a linear relation to the seasonal precipitation of the nearby stations (X) scaled by a proportionality factor (α). The proportionality factor, α is the average slope of the long term MAP for the two reference points. Y is therefore given as $Y = \alpha X$. The rainfall was maintained constant above this elevation to 4,565 m.a.s.l. for Mt. Meru and 5,880 m.a.s.l. for Mt. Kilimanjaro. This assumption is expected to have negligible effect at the Pangani River Basin because of the relative small area above this elevation (3%). Six dummy stations were therefore extrapolated from the existing rainfall stations to the mountain peaks.

River discharges for six gauging stations were obtained from the Pangani Basin Water Office (Moshi, Tanzania), see Fig. 1. The measurements were obtained as daily water level measurements and converted to daily discharge data using their corresponding rating curves equations for the period 2008 - 2010.

3.1.2 Evaporation and soil moisture

The actual evapotranspiration (ET_a) and soil moisture data for the Upper Pangani River Basin were obtained from a recent and related research by Kiptala et al. (2013b). ET_a and soil moisture data for 8-day and 250 m resolutions for the years 2008 - 2010 were derived from MODIS satellite images using the Surface Energy Balance Algorithm of Land (SEBAL) algorithm (Bastiaanssen et al., 1998a; 1998b). Actual evapotranspiration (ET_a) is comprised of interception (I), soil evaporation (E_s), open water evaporation (E_o) and transpiration (T).

3.1.3 Land use and land cover types

In this study, we employed the LULC classification for the Upper Pangani River Basin developed by Kiptala et al. (2013a). They derived the LULC types using phenological variability of vegetation for the same period of analysis, 2008 to 2010. LULC types include 16 classes dominated by rainfed maize and shrublands that constitute half of the area in the Upper Pangani River Basin.

3.1.4 Other Spatial data

Elevation and soil data were also obtained for the Upper Pangani River Basin. A digital Elevation Model (DEM) with 90 m resolution was obtained from the Shuttle Radar Topography Mission (SRTM) of the NASA (Farr et al., 2007). The soil map was derived from the harmonized world soil database which relied on soil and terrain (SOTER) regional maps for Northern and Southern Africa (FAO/IIASA/ISRIC/ISS-CAS/JRC, 2012).

3.2 Model development

The hydrological model was built to simulate stream flow for the period 2008-2010 for the Upper Pangani River Basin. An 8-day timestep and 250-m moderate resolutions has been used to correspond to availability of remotely sensed ET_a data for the period of analysis. The 8-day time step is sufficiently short for the agricultural water use process, which has a timescale range of between 10 - 30 days (unsaturated zone storage over transpiration rate). In addition, this timescale is assumed to be sufficiently large to neglect travel time lag in the river basin. The other general hydrological processes in the river basin are estimated to have larger time scales (Notter et al., 2012). The spatial scale of 250-m is limited by the available MODIS satellite data. This is reasonably representative of the sizes of the small-scale irrigation schemes in the Upper Pangani River Basin.

STREAM, a physically based conceptual model, was developed in the PcRaster modelling environment (Aerts et al., 1999). The PcRaster scripting model environment consists of a wide range of analytical functions for manipulating Raster GIS maps (Karssenberg et al., 2001). It uses a dynamic script to analyze hydrological processes in a spatial environment. The PcRaster environment allows for tailored model development and can therefore be used to develop new models, suiting the specific aims of the research including the availability of field data. The STREAM model in PcRaster environment allows the inclusion of spatially variable information like ET_a and soil moisture in the model. Furthermore, STREAM model is an open source model

which has been applied successfully in other data limited river basins, especially in Africa (Gerrits, 2005; Winsemius et al., 2006; Abwoga, 2012; Bashange, 2013).

In the STREAM model, surface runoff is computed from the water balance of each individual grid cell, which is then accumulated in the local drainage direction derived from DEM to the outlet point (the gauging station). The model structure consists of a series of reservoirs where the surface flows are routed to the rivers. We modified the STREAM model by including an additional blue water storage parameter (S_b) that regulates Q_b in the unsaturated zone. Q_b can be derived from the groundwater as capillary rise, $C(t)$, or river abstraction, $Q_d(t)$. The input variables for the modified STREAM model are: Precipitation (P), Interception (I) calculated on a daily basis as a pre-processor outside the model. Evaporation (E_s, E_o) and Transpiration (T) denoted as $[E + T]$ was derived by subtracting I for the total evaporation (ET_a) derived from SEBAL $[ET_a - I]$. The minimum soil moisture, $S_{u,min}$ is also derived from SEBAL. The other parameters are determined through calibration. Fig. 2 shows the modified STREAM model structure for Upper Pangani River Basin.

<INSERT FIGURE 2>

In the model $E+T$ and the $S_{u,min}$ are the main drivers of the hydrological processes in the unsaturated zone of the model. $E+T$ is the evaporation (soil moisture) depletion component while $S_{u,min}$ is the depletion threshold. It is assumed that excess water from the upstream cells or pixels would supplement water needs of the middle or lower catchments where supplementary water is used. The Upper Pangani River Basin is a typical river basin, where precipitation exceeds ET_a in the upper catchments and hence contributes river flow to the downstream catchments.

The rationale for accounting for Q_b in the model is motivated by the incapability of the original STREAM model if applied in irrigated landscapes to simulate actual transpiration. The original STREAM model was developed specifically for natural landscapes dominated by woody savannas and wetlands with high storage capacity (Dambos) in the Zambezi River Basin (Gerrits, 2005; Winsemius et al., 2006). The blue water use is therefore limited and has been accounted for by the capillary rise only. The total transpiration was therefore derived only as a function of potential evaporation and the soil moisture (from precipitation) in the unsaturated zone using the relation by Rijtema and Aboukhaled (1975). Bashange (2013) using the original STREAM model found that simulated $E + T$ for irrigated croplands were significantly lower compared to SEBAL $E + T$ for dry seasons in the Kakiwe Catchment, Upper Pangani River Basin. The result

was attributed to lower soil moisture levels at the unsaturated zone (not replenished in the model by blue water use).

3.3 Model Configuration

3.3.1 Model input

5 *Interception (I)*

When precipitation occurs over a landscape, not all of it infiltrates into the subsurface or becomes runoff. Part of it evaporates back to the atmosphere within the same day the rainfall takes place as interception. The interception consists of several components that include canopy interception, shallow soil interception or fast evaporation from temporary surface storage

10 (Savenije, 2004). The interception is dependent on the land use and is modeled as a threshold value (*D*). The interception process typically has a daily time scale, although some work has been done to parameterize the interception threshold on a monthly timescale (De Groen and Savenije, 2006).

In our case, we calculate the daily interception according to Savenije, (1997; 2004) outside of the

15 model (see Eq. 1);

$$I_d = \min\left(D_d, P_d\right) \tag{1}$$

Where I_d is the daily interception, D_d daily interception threshold and P_d is the observed precipitation on a rainy day. Since I_d occurs on a daily time step during a precipitation (P_d) event, the interception at 8-day ($I_{d(8)}$) is derived from the accumulated daily interception computed

20 based on daily precipitation. The interception thresholds (D_d) vary per land use and have been adopted from the guidelines provided by Liu and de Smedt (2004) and Gerrits (2010). As such an interception threshold of 2.5 mm day^{-1} was used for croplands and natural vegetation and 4 mm day^{-1} for forest.

Net Precipitation (P$_e$)

25 The net precipitation ($P_{e(8)}$) is calculated by subtracting the accumulated interception ($I_{d(8)}$) from the accumulated precipitation ($P_{d(8)}$) for the 8-day time scale.

$$P_{e(8)} = \sum_{0}^{8} \left(P_d - I_d\right) \qquad \forall_t \tag{2}$$

$P_{e(8)}$ is split through a separation coefficient (c_r) into the two storages, unsaturated and saturated (groundwater) storages. c_r is a calibration parameter that is dependent on the soil type and land

30 use types.

Evaporation depletion (E + T)

The evaporation depletion ($E + T$) is derived by subtracting the interception component of the actual evapotranspiration (ET_a) at each timestep. ET_a from SEBAL includes $I_{d(8)}$ at 8-day time step.

$$5 \quad E + T = \left(ET_a - I_{d(8)}\right) \tag{3}$$

3.3.2 Unsaturated zone

The maximum soil moisture storage ($S_{u,max}$) was defined based on land use and soil types. Water available for evaporation depletion includes water infiltrated from precipitation ($c_r \times P_e$) and blue water use (Q_b), consisting of water from capillary rise (C) and river abstraction (Q_d). During the dry (nonrainy) periods, the spatial variation in soil moisture is controlled by vegetation through the uptake of blue water resources (Seyfried and Wilcox, 1995). The model assumes a minimum soil moisture level ($S_{u,min}$) which varies for managed and natural landscapes. Soil moisture status at each time step (S_u) is therefore a key variable controlling water and energy fluxes in soils (Eq.4 & 5).

$$15 \quad Q_b = E + T \rightarrow if\left(S_u \leq S_{u,min}\right) \tag{4}$$

$$Q_b = 0 \rightarrow if\left(S_u > S_{u,min}\right) \tag{5}$$

As a result the green water use is defined as the evaporation depletion less the blue water use (Eq. 6).

$$Q_g = E + T - Q_b \tag{6}$$

The value for $S_{u,min}$ for each land use type is assumed to be realized during the dry months and is expressed as a fraction of $S_{u,max}$ (soil moisture depletion fraction). $S_{u,min}$ is derived in the SEBAL model for dry months as an empirical function of the evaporative fraction, Λ (the ratio of the actual to the crop evaporative demand when the atmospheric moisture conditions are in equilibrium with the soil moisture conditions) (Ahmed and Bastiaanssen, 2003), see Eq. (7).

$$25 \quad f = \frac{S_{u,min}}{S_{u,max}} = e^{(\Lambda-1)/0.421} \tag{7}$$

where f is the soil moisture depletion fraction expressed as a fraction of soil moisture, $S_{u,min}$ to the moisture value at full saturation, $S_{u,max}$ for the dry months. $S_{u,min}$ was realized in the month

January, which is the driest period in the river basin. Values for *f* are given in Fig. 3 for selected land use types for the dry month of January averaged over 2008-2010.

<center><INSERT FIGURE 3></center>

The soil moisture levels agree reasonably well with previous field studies that have shown similar ranges for natural land use types in sub humid and semi - arid areas (Fu et al., 2003; Korres et al., 2013). It is also noted that the SEBAL model has some level of uncertainty to soil moisture storage and water stress (Ruhoff et al., 2012). In recognizing this uncertainty, the modified SEBAL model also uses a water balance approach where lower $S_{u,min}$ levels can be tolerated with respect to the available Q_b during the dry season for natural land use types.

3.3.3 Saturated zone

Apart from the net precipitation component (($1-c_r$)×P_e), the saturated zone receives water from the unsaturated zone when the soil moisture S_u reaches field capacity ($S_{u,max}$). Excess overflow (Q_u) is routed to the groundwater using a recession factor, K_u. The saturated zone consists of three linear outlets which are separated by $S_{s,min}$ to represent the minimum storage level, $S_{s,q}$ to represent quickflow threshold and $S_{s,max}$ to represent rapid subsurface overflow. The flows are routed using K_o, K_q and K_s calibration coefficients respectively.

When the groundwater storage (S_s) exceeds the $S_{s,max}$, then saturation overland flow (Q_o) occurs:

$$Q_o = \max\left(S_s - S_{s,\max}, 0\right)/K_o \tag{8}$$

where K_o is the overland flow recession constant.

The second groundwater flow component is the quick groundwater flow (Q_q). It is assumed to be linearly dependent on the S_s and a quick flow threshold $S_{s,q}$ determined through calibration (Eq. 9).

$$Q_q = \max\left(S_s - S_{s,q}, 0\right)/K_q \tag{9}$$

where K_q is the quick flow recession constant.

The third component is the slow groundwater flow ($Q_{s,g}$) which is dependent on the S_s levels

$$Q_{s,g} = \left(S_s\right)/K_s \tag{10}$$

where K_s is the slow flow recession constant.

K_o, K_q, K_s equal to 1, 2 and 28 respectively and were determined from recession curve analysis (where 1 unit is equal to the 8-day time step).

The maximum saturation storage ($S_{s,max}$) is a key variable that determines the dominant hydrological processes in the saturated zone. Three hydrological zones can be delineated from $S_{s,max}$, i.e. wetland, hill-slope and snow/ ice zone. When $S_{s,max}$ is low, the saturation excess overland flow is dominant. This is characteristic for wetland systems described in detail by Savenije (2010). It occurs in the low lying areas of the Pangani river basin where slopes are modest, or with shallow groundwater levels. During a rainfall event, there is no adequate storage of groundwater leading to saturation excess overland flow. The wetland system is therefore dominated by Q_o and as such the $S_{s,max}$ is set very low or at zero (fully saturated areas) and c_r at 1. As the elevation and slope increases, the groundwater depth as well as the $S_{s,max}$ increase gradually. This is characteristic of the hill-slope system where storage excess subsurface flow is the dominant runoff mechanism. Topographic indicators can be used to identify and separate this zone from the wetland system (where $S_{s,max}$ is near zero). Recently developed indices that can be used include the elevation above the nearest open water (H) (Savenije, 2010), or the Height Above the Nearest Drainage (HAND) (Nobre et al., 2011; Cuartas et al., 2012). The first topographic indicator, H (elevation above the nearest open water) is used in this study. H is derived from the level where groundwater storage is low or near zero. This was estimated from 92 groundwater observation levels located in the lower catchments of the river basin (Fig. 4).

Fig. 4 shows the delineation of the dominant hydrological processes in the Upper Pangani River Basin, including the wetland and hillslope (includes snowmelts at the peak of the mountains).

<center><INSERT FIGURE 4></center>

$S_{s,max}$ is not completely available for groundwater storage due to the soil texture (porosity and soil compression). According to Gerrits (2005), the maximum groundwater storage, $S_{s,max}$ [mm] for hillslope can be estimated using the natural log function of water storage depth, H_s (Eq. 11).

$$S_{s,\max} = 25 \times \ln H_s \tag{11}$$

where H_s [m] is the normalized DEM above H (where active groundwater storage is assumed zero). It is noteworthy that the wetland system can still exist along the drainage network of river system beyond H. This is possible since the H_s would still ensure a low groundwater storage ($S_{s,max}$) which makes the wetland system the dominant hydrological process. As observed in Fig. 4, the middle catchment forms the transition from the wetlands to the hillslope. It is noted that the hydrological landscape, plateau (dominated by deep percolation and hortonian overland flow) described in detail by Savenije (2010) is not existent on the slopes of Kilimanjaro and Meru, the

higher elevations are forested and is active in the rainfall - runoff process. It is therefore modeled as forested hillslope.

The third zone delineated is the snowmelt. The amount of snow in the river basin is limited to the small portion of the mountain peaks of Mt. Kilimanjaro and Mt. Meru. The snowmelt occurs at elevation ranges of 4,070 m.a.s.l to 5,880 m.a.s.l and is derived from the land use map (Kiptala et al., 2013a). During rainfall seasons, the snow is formed and stored in the land surface. During the dry season, the snow melts gradually to the soil moisture and to the groundwater. This is unlike the temperate climate where a lot of snow cover is generated during the winter seasons which may result in heavy or excess overland discharge during the summer seasons. Furthermore, Mt. Kilimanjaro has lost most of its snow cover in the recent past due to climate variability / change, with significant snow visible only on the Kibo Peak (Misana et al., 2012). According to Grossmann (2008) the snowmelt contribution to groundwater recharge is insignificant in the Kilimanjaro aquifer. Simple representation of snowmelt can therefore be made using the hillslope parameters where the precipitation is stored in the unsaturated zone ($c_r = 1$ for snow) as excess unsaturated storage. The snowmelt is thereafter routed by K_u (unsaturated flow recession constant) to the groundwater over the season. This model conceptualization enables the hydrological model to maintain a limited number of parameters.

3.3.4 Interaction between the two zones

Capillary rise only occurs when groundwater storage is above a certain level, $S_{c,min}$. $S_{c,min}$ can be a fixed or a variable threshold value of the groundwater storage (S_s). Winsemius et al. (2006) adopted a fixed value of 25 mm as the $S_{c,min}$ for the Zambezi River basin. Since $S_{s,max}$ (from Eq. 11) is a function of H_s, a fixed threshold is not possible in this study. $S_{c,min}$ is made a function of groundwater storage S_s to provide a spatially variable threshold through calibration over the river basin. Capillary rise above this threshold is estimated on the basis of the balance between water use needs at the unsaturated zone and water availability in the saturated zone. Actual capillary rise is determined implicitly using the maximum capillary rise C_{max} (calibration parameter for each land use type), evaporation depletion ($E + T$) and the available groundwater storage S_s. Below $S_{c,min}$, a minimal capillary rise C_{min} is possible and is assumed to be zero for this study (timescale of 8-day is assumed low for substantial C_{min} to be realized).

$$C = \min \left(C_{max}, (E + T), S \right) \rightarrow if \left(S_s \geq S_{c,min} \right) \tag{12}$$

where the active groundwater storage for capillary rise, $S = S_s - S_{c,min.}$

However, since the capillary flow is low compared to water use for some land use types, supplementary blue water from river abstractions (Q_d) is required in the system. The third blue water storage term S_b, is introduced to regulate blue water availability from capillary rise, C, and river abstractions, Q_d. River abstractions include water demands from supplementary irrigation, wetlands and open water evaporation for lakes or rivers derived directly from the river systems.

$$Q_d = (Q_b - C) \rightarrow if\,(S_b \leq Q_b) \tag{13}$$

$$Q_d = 0 \rightarrow if\,(S_b > Q_b) \tag{14}$$

where Q_b is the blue water required to fill the evaporation gap that cannot be supplied from the soil storage. For irrigated croplands, Q_d is assumed to represent the net irrigation abstractions in the river basin. The assumption is based on the 8-day timestep that is considered sufficient for the return flows to get back to the river systems, i.e. the flow is at equilibrium. Q_d is therefore modeled as net water use in the river system.

Since river abstractions mainly occur in the middle to lower catchments and the accumulated flow would have a resultant net effect equivalent to the total simulated discharge, Q_s at a downstream outlet point or gauge station (Eq. 15 and 16).

$$Q_{s1} = Q_o + Q_q + Q_{s,g} \tag{15}$$

$$Q_s = Q_{s1} - Q_d \tag{16}$$

3.4 Sensitivity and uncertainty analysis

Since a number of assumptions were introduced to simulate the hydrological processes in the basin, a sensitivity analysis was performed to assess the influence of model input parameters to the variation of model performance. The parameter adjustments were done during the calibration process manually by trial and error. Some parameter values where manually altered within parameter ranges while others were calibrated freely. According to Lenhart et al. (2002), the parameter sensitivity can be achieved by varying one parameter at a time within the parameter range or using a fixed percentage change of the base value while holding the others fixed. Three parameter values; interception threshold (D), separation coefficient of net precipitation between the unsaturated and saturated zones (c_r) and the quick flow components (q_c) were varied within the parameter ranges. Three parameter values for maximum storage in the unsaturated zone ($S_{u,\,max}$), maximum storage in the saturated zone ($S_{s,\,max}$) and maximum potential capillary rise (C_{max}) that were calibrated freely were varied by a fixed change of the base value. The other three

14

parameter values representing runoff timescales (K_o, K_q, K_s) were also varied by a fixed value from the estimates determined from the recession curve.

A sensitivity coefficient was computed to represent the change in the response variable that is caused by a unit change of an input variable, while holding the other parameters constant (Gu and Li, 2002). The sensitivity coefficient (SC) was normalized by reference values representing the range of each output and input variables to give the sensitivity index (SI) represented by Eq. (17).

$$SI = \left(\frac{y_i - y_0}{x_i - x_0} \right)\left(\frac{x_i + x_0}{y_i + y_0} \right) \tag{17}$$

where x_0 and y_0 are the base input parameter value and model output from the final model calibration respectively; x_i and y_i are the varied input parameter and the corresponding model output, respectively. SI makes it feasible to compare the results of different input parameters independent of the chosen variation range (Lenhart et al., 2002; Bastiaanssen et al., 2012). The SI can be positive or negative depending on the co-directional response of the model performance to the input parameter change. The absolute higher SI values indicate higher sensitivity.

3.5 Model Performance

The modified STREAM model was calibrated and validated against measured daily discharge data from five gauging stations in the basin (see Fig. 1). One discharge gauge station, 1dd55, had a lot of missing data. Nevertheless, the limited information from this station, most upstream and the only one in the upper Mt. Meru, was useful in the calibration process of the downstream gauge stations. The daily discharge data were aggregated to 8-day time scale for the period 2008 - 2010. Since the secondary data from remote sensing (ET_a and f) were available for only 3 years, 1 year of data was used for calibration while the remainder of 2 years data used for the validation. An initial 1 year (46 simulations) was used as warm-up period to stabilize the model parameter using the mean input values. In total, the model was simulated for 184 time steps (4-year period).

The following goodness to fit statistics were used to evaluate the model performance. The Nash-Sutcliffe model efficiency coefficient (E_{ns}) (Nash and Sutcliffe, 1970), Mean Absolute Error (MAE) and the Relative Mean Square Error (RMSE) in Eq. (18), Eq. (19) and Eq. (20) respectively.

$$E_{ns} = 1 - \frac{\sum_{i=1}^{n} (Q_s - Q_o)^2}{\sum_{t=1}^{n} (Q_o - \bar{Q}_o)^2} \qquad (18)$$

where Q_s and Q_o are simulated discharge and observed discharge, $\bar{Q}_o$ is the mean of the observed discharge and n is the discharge data sets (n = 46 calibration; n = 92 validation)..

$$MAE = \frac{1}{n} \sum_{i=1}^{n} |Q_s - Q_o| \qquad (19)$$

5
$$RMSE = \sqrt{\frac{\sum_{i=1}^{n} (Q_s - Q_o)^2}{n}} \qquad (20)$$

Since the model priority objective is to simulate low flows, the E_{ns_ln} was also evaluated using natural logarithm of the variables in Eq. (18). The E_{ns} values range $[-\infty, 1]$, with 1 being the optimum (Ehret and Zehe, 2011). The range of MAE and RMSE is $[0, \infty]$, with zero being the optimum (Murphy, 1995). The model is optimized using these parameters to achieve a balance

10 between the correlation, the bias, and the relative variability in the simulated and observed discharge (Gupta et al., 2009). The model estimates for irrigation water use ($Q_{b(I)}$) were also compared with the field data on net irrigation water use from the river basin agency, Pangani Basin Water Office.

3.6 Scenario development

15 In Pangani River Basin, blue water use is currently over-exploited (Kiptala et al., 2013b). The implication for additional water allocation on stream flow to the nationally important hydropower stations needs to be known. This may also result in water savings or tradeoffs with other interventions or water uses. The crop yields for rainfed and supplementary irrigated lands are also low leading to low crop water productivity (Makurira et al., 2010). A few water

20 management scenarios targeted on water savings and improved crop water productivity is explored using the modified STREAM model. They include i) Water saving through increased irrigation water efficiency, ii) increased crop productivity for rainfed lands, and iii) modifying the landscape for increased agricultural production.

To meet the first objective, the non-beneficial component of evaporation (soil evaporation) for

25 irrigated landscapes is targeted for reduction. Soil evaporation (E_s) can account to up to 40% of evaporation depletion ($E+T$) in irrigated landscapes (Bastiaanssen et al., 2012; Burt et al., 2001).

16

In Pangani River Basin, located in the tropical climate, the irrigation system used by smallholder farmers that conveys water using small earthen furrow canals may have high levels of E_s. It is noteworthy that interception (I) also includes shallow (fast) soil evaporation that is implicitly derived only from precipitation. For demonstrative purposes, a reduction of 5% in $E + T$ for supplementary irrigated mixed crops is targeted (Scenario 1). The reduction represents about 15% of E_s if we assume a conservative E_s of 30% of $E + T$ in the supplementary irrigation systems. There are several methods for reducing E_s. They may include the lining of the main canals or using more efficient micro-irrigation systems. Further reduction can also be achieved by either straw or mechanical mulching (Prathapar and Qureshi, 1999; Zhang et al., 2003).

To meet the second objective, productive transpiration for rainfed maize (highland) is increased by 30% (Scenario 2a). According to Makurira et al. (2010), the crop water productivity for smallholder rainfed farms can be improved by using systems innovations (SIs). The study was done in Makanya catchments within the Pangani River Basin. The SIs used combined runoff harvesting with in-field trenches and soil bunds which resulted in an increase of transpiration of 47%. The SIs aimed also at preventing soil and nutrient loss. An increase in T would result in an increase in biomass production and thus crop yields (Steduto et al., 2009). The rainfed maize in the highland areas was targeted due to the relative high precipitation during the rainy seasons. In-field trenches and soil bunds (*Fanya juus*) is normally associated with high infiltration levels and higher soil moisture retention (Kosgei et al., 2007; Makurira et al., 2010). An additional increase in $S_{u,max}$ of 30% is also investigated in addition to the increased transpiration for highland rainfed maize and coffee (Scenario 2b).

For the third objective, the area for irrigated sugarcane is doubled to its potential (Scenario 3). Currently, TPC irrigation scheme covers an area of 8,000 ha, for which 7,400 ha is under sugarcane cultivation with the reminder providing the irrigation services. The potential irrigation area is estimated at 16,000 ha constrained by limited water resources. The expansion of the irrigation system is of great interest in the basin due to the high sugar demand and increasing potential for bio-fuels.

4 Results and discussion.

4.1 Calibration and validation results

Figs. 5 & 6 show the comparison of the observed and simulated hydrographs and the average precipitation for five outlets (gauge stations) in the Upper Pangani River Basin. The figures

17

provide a visual inspection of the goodness of fit of the data with an additional scatter plot for the most downstream outlet (1dd1). The model simulates the base flows very well both during the calibration and validation periods. The peak flows for the larger streams (1dd54, 1dd1) were better simulated than for the smaller streams (1dc8a, 1dc5b, 1dc11a). It is to be noted that the observed discharge data is also subject to uncertainty which is more pronounced for the smaller streams. The remotely sensed data, ET_a and f also have a higher uncertainty during the rainy season (peak flow season). This is the period when most clouded satellite images exist and the cloud removal process is subject to uncertainty (Kiptala et al., 2013b).

<center><INSERT FIGURE 5></center>

<center><INSERT FIGURE 6></center>

Table 1 shows the performance model results for the validation and calibration of the modified STREAM model in the Upper Pangani River Basin. The Nash-Sutcliffe Efficiency, E_{ns} for the calibration period scored > 0.5 (except 1dd11a = 0.46) which is indicative of good model performance. In the validation period, two outlet points had scores < 0.5 (1dd11a - 0.33 and 1dd54 - 0.42) which indicates a moderate performance. The Nash-Sutcliffe Efficiency for natural logarithm, E_{ns_ln}, which emphasizes the base flow, resulted in better results with all outlet points scoring ≥ 0.6. There was a slight reduction in E_{ns_ln} in outlet points 1dd54 (calibration) and 1dd8a, 1d5b (validation) but overall the model performance on the low flows was good.

<center><INSERT TABLE 1></center>

MAE ranged between 0.62 m^3 s^{-1} and 2.08 m^3 s^{-1} for the larger streams in the calibration period. A big difference is observed between the RMSE and MAE (up to four times) for the downstream stations 1dd54 and 1dd1 during the calibration period. The result is indicative of large (noisy) variations between the simulated and observed discharges. Fig. 5 also shows that the large deviations arise during the rainy periods (Masika and Vuli seasons). This may be attributed to the uncertainties of the remote sensing data in the clouded periods (rainy days). Such uncertainties can be avoided by using passive microwave imagery (Bastiaanssen et al., 2012). Furthermore, the river gauging stations are poorly maintained in the river basin. The discharge rating curves are also not regularly updated despite the changes in the river regime. Model conceptualization assumptions such as irrigation water use and return flows may also not coincide in space and time with the actual processes in the river basin. Errors in boundary conditions on the representation of groundwater may also occur if they do not coincide with the river systems.

4.2   Sensitivity Analysis

The sensitivity analysis of the input parameters is given in Table 2. The sensitivity index (SI) was analyzed using the RMSE and MAE model performance indicators for the entire simulation period using the discharge measurements at outlet point (1dd1). The base input values (x_0) were the final calibrated values that were varied by a fixed or percentage change (x_1 or x_2). Decrease in $S_{u,max}$ by 25% resulted in the highest SI of -1.97 for RMSE. However, a similar increase of 25% did not have any significant change in model output. The sensitivity is mainly attributed to the overland flow that is influenced by the water storage in the unsaturated zone. Similar changes in $S_{s,max}$ also resulted in moderately high sensitivity for both RMSE and MAE. This is mainly because the saturated zone controls all the runoff components. Separation coefficient c_r that separates the net precipitation between unsaturated and saturated zones and the quick flow coefficient, q_c had high sensitivity. The values used $c_r = 0.75$ and $q_c = 0.75$ (aggregated averages) for various land use types were generally derived from previous modelling experiences and where based on the soil type and land use.

The soil moisture depletion fractions (f) were derived from the SEBAL model for various land use types. An aggregated average f value of 0.33 was adopted from the mean values for the land use types that ranged between 0.2 for natural land use types to over 0.6 for irrigated agriculture (also see Figure 3). These parameters resulted in minimum sensitivity since the ranges used (±25% of the base values) where reasonable within the derived estimates from remote sensing.

The runoff timescales parameters K_o and K_q also had low sensitivity because the flow times were short and within the estimates derived from the recession curves. The timescale K_s for slow groundwater flow that has a higher flow times had a moderate sensitivity. A lower timescale for K_o of 1 time step (8-days) may introduce some uncertainty if the model was used to simulate flood events that are critical at shorter timescales of 1 - 2 days. However, for hydrological processes that characterize agricultural water use such as irrigation scheduling or dry river flows, the uncertainty is minimal.

The maximum capillary rise (C_{max}) was calibrated through a water balance process to maintain the evaporation depletion ($E + T$). An aggregated average value of 2 mm day^{-1} was achieved and ranged between 1.1 mm day^{-1} for woodland landscape in semi-arid areas to a maximum of 2.8 mm day^{-1} in the natural dense forest in humid climate. The calibrated values were within the ranges for natural vegetation reported in literature (Shah et al., 2011). In natural and rainfed

19

systems, only C_{max} was calibrated to maintain the evaporative capacity of the unsaturated zone. The actual capillary rise (C) would not change with an increase in C_{max}. However, a decrease in C_{max} would constrain C, thus resulting in lower soil moisture conditions in the unsaturated zone. For irrigated land use types, the evaporative capacity ($E + T$) is maintained by both C and irrigation (Q_d). The changes in C due to high or lower C_{max} threshold will correspond to a similar change in Q_d. C_{max} was therefore a less influential parameter with low sensitivity in natural vegetation. Interception threshold, D showed also low sensitivity to changes within the parameter range. D was computed on a daily basis using the interception threshold for various landuse types derived from literature. However, the actual interception is more dependent on the daily variability of rainfall than the total interception threshold. Similar findings were observed by De Groen and Savenije (2006). While the interception threshold is not an influential parameter, actual interception (I) is still important water balance component as the water for the other processes is dependent on the net precipitation after interception (Makurira et al., 2010).

<INSERT TABLE 2>

4.3 Model interpretation

4.4 Interception and Evaporation depletion

There is general consensus that actual interception (I) is a key component in hydrology and water management. I influences the net precipitation and therefore the amount of water available for evaporation ($E+T$). Evaporation depletion ($E+T$) influences the stream flow dynamics and is the manageable component of ET_a in biomass production. Therefore, there is a need to distinguish $E+T$ from the calculated I as a deficit of total ET_a (SEBAL), Fig. 7.

<INSERT FIGURE 7>

The mean annual I ranged between 8 - 24% of the total evapotranspiration. The land use types in the upper catchments, e.g. forest, rainfed coffee and bananas, had higher I. Irrigated sugarcane and natural shrublands located in the lower catchments had lower I. The variation is mainly influenced by the maximum threshold (D) and the rainfall (intensity and frequency) which are relatively higher for land use types in the upper catchments. The forest interception average estimate of 24% of the total evapotranspiration (or 22% of the total rainfall) is comparable with field measurements from previous studies that found forest canopy interception of about 25% of the total rainfall in a savannah ecosystem in Africa (Tsiko et al., 2012).

Q_b contributions, e.g. irrigation, also enhanced the evaporation depletion ($E+T$) component of ET_a resulting in relatively lower I for irrigated croplands. Any intervention to change I would influence antecedent soil moisture conditions especially during small rainfall events (Zhang and Savenije, 2005). This may influence the productivity of $E+T$ and / or the stream flow generation in the river basin. However, more research is required to estimate explicitly the changes in I from certain field based interventions. The outcome of such studies maybe incorporated in the STREAM model.

4.5 Blue and green water use.

Figs. 8(c) and 9 shows the resultant blue water use (Q_b) and the direct contribution of precipitation (Q_g) to the ET_a (actual evapotranspiration) for various land use types. Q_b is closely related to the land use and the ET_a as observed in Figs. 8(a) & 8(b). Water bodies (lakes and reservoir) and the wetlands have the highest Q_b, contributed by the high open water evaporation. The average Q_b for water bodies is approx. 56% of the ET_a with a maximum of 74% (1,642 mm yr^{-1}) observed at the lower end of the NyM reservoir. The Q_b is high in the NyM reservoir because of the high potential evaporation attributed to hotter climatic conditions and lower precipitation levels in the lower catchments. Wetlands and swamps located in the lower catchments also resulted in high Q_b of approximately 42% of ET_a. In irrigated croplands, the Q_b was also moderately high with a range of between 20% for irrigated mixed crops and bananas in the upper catchments, and 44% for irrigated sugarcane in the lower catchment.

Rainfed crops and natural vegetation including the forests had a lower Q_b, mainly stemming from groundwater (and snow melts). Sparse vegetation, bushlands, grasslands, natural shrublands had Q_b contributions of less than 1% of total ET_a, while rainfed maize (middle catchments) and rainfed coffee (upper catchments) had Q_b contributions of 2% and 7% of ET_a respectively. Dense forest and Afro-Alpine forest had slightly higher Q_b contributions (ranging between 7 - 9 %) attributed mainly to the availability of groundwater from snow melts in the upper mountains.

Notable higher Q_b was experienced in the dry year of 2009 (as shown by the error bars in Fig. 9). This is attributed to higher potential evaporation from relatively drier weather conditions. The lower precipitation during this period also resulted in increased groundwater use for the afro-alpine and dense forest land uses in the upper catchments. For instance the Q_b contribution to ET_a for dense forest increased from 5% in 2008 (a relatively wet year) to 10% in 2009. The enhanced Q_b for the irrigated croplands during 2009 is also attributable to the higher potential

evaporation and limited precipitation that increased the irrigation water requirement. This is illustrated by irrigated sugarcane where Q_b increased from 35% in 2008 to 55% in 2009. Q_b for supplementary irrigation also increased from 14% to 29% during the dry year. The Q_b for year 2010 was in general average for all land use types which is indicative of the average weather conditions that prevailed during the year.

<center><INSERT FIGURE 8></center>

<center><INSERT FIGURE 9></center>

4.6 Irrigation water use

This section presents the model results for supplementary irrigation water use ($Q_{b(I)}$) as estimated at various outlet points (gauging stations) in the river basin. The annual irrigation abstractions, predominant during dry seasons, were accumulated and the average mean for the period 2008-2010 is presented in Fig.10. Six gauge stations and three additional points (accumulation points for Kikuletwa, Ruvu and Lake Jipe) were also considered. The annual net irrigation (in million cubic meters) was converted to m^3 s^{-1} to allow easier comparison with the discharge data in section 4.1.

<center><INSERT FIGURE 10></center>

The $Q_{b(I)}$ ranges from 0.06 m^3 s^{-1} on the smaller streams to a total of 3.4 m^3 s^{-1} and 4.2 m^3 s^{-1} in the outlets of the Ruvu and Kikuletwa river systems respectively. A significant irrigation abstraction of 1.5 m^3 s^{-1} was observed by the TPC sugarcane irrigation system, the largest single irrigation scheme in the river basin. The total $Q_{b(I)}$ upstream of NyM reservoir was estimated at 7.6 m^3 s^{-1}, which represents approximately 50% of the low flows in the Upper Pangani River Basin.

Open canal irrigation is the commonly used irrigation technique in the Upper Pangani River Basin. There are an estimated 2,000 small-scale traditional furrow systems, some 200 - 300 years old (Komakech et al., 2012). According to records at the Pangani Basin Water Office, approximately 1,200 of these abstractions have formal water rights. PWBO estimates that the total gross irrigation abstraction is approximately 40 m^3 s^{-1}. The irrigation efficiencies of the irrigation systems range between 12 - 15% (Zonal Irrigation office, Moshi). Here, we adopted higher irrigation efficiency limit of 15% to compensate for any uncertainties that may arise from the higher irrigation efficiencies in the larger irrigation schemes. The field estimates provides net irrigation consumptions of approximately 6 m^3 s^{-1} (using 15% efficiency) and about 79% of the

<center>22</center>

$Q_{b(I)}$ model estimates (19% efficiency). The water leaks in the traditional furrow canals flows back to the river system. The capacity and ability of the river basin authority to monitor actual water abstraction is limited. However, considering these uncertainties, the modeled net irrigation abstraction was reasonably close to field net irrigation estimates for the Upper Pangani Basin.

4.7 Open water evaporation

The blue water use by the water bodies ($Q_{b(w)}$) upstream of NyM reservoir was also estimated using the modified STREAM model. $Q_{b(w)}$ is the net open water evaporation from blue water which would otherwise flow into the NyM reservoir. The water bodies considered include wetlands (98 km^2), Lake Jipe (25 km^2) and Lake Chala (4 km^2). The total mean $Q_{b(w)}$ were estimated to be 53.6×10^6 m^3 yr^{-1} (1.7 m^3 s^{-1}) and 22.1×10^6 m^3 yr^{-1} (0.7 m^3 s^{-1}) in the Ruvu and Kikuletwa river systems, respectively. The total $Q_{b(w)}$ (12% of low flows) may also provide an insight into ecosystem services or benefits provided by the natural water bodies compared with the alternative uses, such as irrigation or hydropower in the downstream part of the river basin.

4.8 Future water management scenario using modified STREAM model

The previous sections illustrate how the modified STREAM model provides spatial information on the water use (green and blue) under current situation. The information is useful especially in monitoring unregulated irrigation water use. The model also provided useful information on the implication of future water use management scenarios in the river basin. Table 3 shows the real impact of the interventions on the water resources under the scenarios defined in section 3.6. The changes in surface runoff were evaluated from the outlet points (1dc & 1dd) upstream of NyM reservoir, Upper Pangani River Basin (Fig. 10).

<INSERT TABLE 3>

If soil evaporation is reduced in irrigation systems (Scenario 1), real water saving of 37.8×10^6 m^3 yr^{-1} can be achieved. The additional water saved (4% of total river flow), mostly groundwater flow can be utilized in the expansion of the irrigated sugarcane (scenario 3). Scenario 1, alternatively, could also release additional base flow that may be required for other water uses that include environmental and / or downstream hydropower demands. Financing of the required interventions can also form a basis for basin-wide trade-off negotiations between downstream and upstream water users.

Scenario 2(a) investigates the implications of up scaling system innovations (SIs) for the rainfed maize cultivated in the highlands. In the area targeted, mixed farming of maize and coffee is

practiced, and covers an area of 72,300 ha (Kiptala et al., 2013a). Half of this area is under maize cultivation. This intervention would result in additional water use of 84×10^6 m^3 yr^{-1}, which is about 10% of the total river flows. The model simulation shows that the water use will be derived from base flow. However, small-scale runoff harvesting devices can be used to store overland flow to supplement blue water needs during the dry seasons. Scenario 2(b) shows that an increase in both T and $S_{u,max}$ would result in slightly higher overland flow water use. This will not only increase water availability in the unsaturated zone for transpiration, but also reduce the soil and nutrient losses normally associated with higher overland flows.

In scenario 3, the increase in the sugarcane irrigated area by 7,400 ha required an additional 53.9 Mm^3 yr^{-1} in average of base flow. The volume required for each year: 45.6 Mm^3 yr^{-1} (2008), 68.6 Mm^3 yr^{-1} (2009) and 47.4 Mm^3 yr^{-1} (2010) varied with the climate conditions. This is about 4%, 11% and 6% of the total river flows in 2008, 2009 and 2010 respectively. An additional conveyance and drainage losses may increase the net water use. It was also observed that the total additional blue water required in scenario 3 is consistent with the current irrigation water use (Q_b) by the existing irrigation system.

5   Conclusions

This paper presents a novel method of developing a spatially distributed hydrological model using blue and green water use at pixel scale. This methodology allows for unprecedented insights into hydrological processes at smaller scales of land use classes. The hydrological model was developed for a heterogeneous, highly utilized and data scarce landscape with a sub-humid and arid tropical climate. The blue water use was quantified by employing a time series of remotely sensed evapotranspiration data as input in STREAM model. The model was also constrained by satellite-based soil moisture estimates that provided spatially (and temporally) realistic depletion levels during the dry season. To further enhance model parameter identification and calibration, three hydrological landscapes wetlands, hill-slope and snowmelt, were identified using topographic data and field observations. Unrealistic parameter estimates, found for example in natural vegetation either through overestimation of satellite-based data or model structure, were corrected in the model conceptualization through the water balance (at pixel scale). The modified STREAM model provided a considerably good representation of supplementary blue water use, which is dominant in the Upper Pangani River Basin.

The model performed well on discharge, especially in the simulation of low flows. The Nash-Sutcliffe coefficient (E_{ns_ln}) ranged between 0.6 to 0.9 for all outlet points in both calibration and validation periods. At the outlet, the model performance was best (E_{ns_ln} = 0.90). The large difference between MAE and RMSE was indicative of large errors or noisy fluctuations (see Figs. 5 & 6) between actual and simulated discharges during the rainy seasons. This was mainly attributed to the uncertainties of the remote sensing data during clouded periods. The uncertainties may also have been exacerbated by possible errors in the hydro-meteorological data and model conceptualization. Model parameters that were freely calibrated for different land use such as maximum unsaturated and saturated storages ($S_{u,max}$, $S_{s,max}$), separation coefficient (c_r) and quick flow coefficient (q_c) resulted in high sensitivity. The model calibration of these parameters can be improved in future by field measurement or by analytical relationships.

The simulated net irrigation abstractions were estimated at 7.6 m^3 s^{-1} which represents approximately 50% of low flows. Model results compared reasonably well with field estimates with less than 20% difference. In addition, the model yields spatially distributed data on net blue water use that provides insights into water use patterns for different landscapes under different climate conditions. Blue water use (Q_b) contribution to ET_a during a dry year (2009) increased from 5% to 10% for dense forest, 35% to 50% for the wetlands and irrigated sugarcane, and 14% to 28% for supplementary irrigation compared to the wet year (2008). Three water management scenarios on water saving and increased crop productivity were also explored using the STREAM model. Reduced soil evaporation of 15% on supplementary irrigation system would result in real blue water savings of 37.8×10^6 m^3 yr^{-1} (4% of total river flows). The water saving could alternatively be used to expand the existing sugarcane irrigation scheme (7,400 ha on sugarcane) that required 6% of total river flows if its area is doubled. Up-scaling of systems innovation for highland rainfed crops to achieve a 30% increase in productive T resulted in additional blue water requirement of 84×10^6 m^3 yr^{-1}. The additional water requirement can be generated from runoff harvesting and storage to save on the already over-exploited blue water resources. This information may form a basis for socio-economic trade-off analysis on the basis of which various basin strategies and financial mechanisms can be formulated for efficient, equitable and sustainable water resources management at the river basin.

The development of advanced methods of generating more accurate remotely sensed data should go hand in hand with ways to improve distributed hydrological models. Such methods may

include the use of passive microwave imagery to generate cloud free ET_a estimates (Bastiaanssen et al., 2012). Future modelling improvements should also aim at simulating the model for longer time series using long term rainfall and RS data (evapotranspiration and soil moisture). The data could be based on stochastic or probabilistic techniques (Salas et al., 2003). In so doing, data can

5   be interpreted in a way that is useful for management and decision-making.

Acknowledgements

References

Abwoga, A. C.: Modeling the impact of landuse change on river hydrology in Mara river basin, Kenya, Master's thesis, UNESCO-IHE Institute for Water Education, Delft, 2012.

20   Aerts, J. C. J. H., Kriek, M., and Schepel, M.: STREAM (Spatial tools for river basins and environment and analysis of management options): set up and requirements. Physics and Chemistry of the Earth, Part B: Hydrology, Oceans and Atmosphere, 24(6), 591-595, 1999.

Ahmed, M. D., and Bastiaanssen, W.G.M.: Retrieving soil moisture storage in the unsaturated

25   zone from satellite imagery and bi-annual phreatic surface fluctuations. Irrigation Systems, 17(2), 3-18, 2003.

Allen, R. G., Tasumi, M., and Trezza, R.: Satellite based energy balance for mapping evapotranspiration with internalized calibration (METRIC): Model. ASCE J. Irrigation Drainage Engineering, 133(4), 380-394, 2007.

Bashange, B. R.: The spatial and temporal distribution of green and blue water resources under different landuse types in the Upper Pangani River Basin, Master's thesis, UNESCO-IHE Institute for Water Education, Delft, 2013.

Bastiaanssen, W. G. M., Cheema, M. J. M., Immerzeel, W. W., Miltenburg, I. J., and Pelgrum H.: Surface energy balance and actual evapotranspiration of the transboundary Indus Basin estimated from satellite measurements and the ETLOOK model, Water Resources Research, 48, W11512, doi:10.1029/2011WR010482, 2012.

Bastiaanssen, W. G. M., Menenti, M., Feddes, R. A., and Holtslag, A. A. M.: A remote sensing Surface Energy Balance Algorithm for Land (SEBAL) 1. Formulation. Journal of Hydrology, 212-213, 198 - 212, 1998a.

Bastiaanssen, W. G. M., Pelgrum, H., Wang, J., Ma, Y., Moreno, J. F., Roerink, G. J., and Van der Wal, T.: A remote sensing Surface Energy Balance Algorithm for Land (SEBAL) 2. Validation. Journal of Hydrology, 212-213, 213-229, 1998b.

Burt, C. M., Howes, D. J., Mutziger, A.: Evaporation Estimates for Irrigated Agriculture in California. ITRC Paper P 01-002. Irrigation Training and Research Center, San Luis Obispo, CA, 2001.

Campo, L., Caparrini, F., and Castelli, F.: Use of multi-platform, multi-temporal remote sensing data for calibration of a distributed hydrological model: an application in the Arno basin, Italy. Hydrological Processes 20, 2693-2712, 2006.

Chang, M., and Lee, R.: Objective double mass analysis. Water resources research, 10(6), 1123-1126, 1974.

Cheema, M. J. M., and Bastiaanssen, W. G. M.: Local calibration of remotely sensed rainfall from TRMM satellite for different periods and spatial scales in the Indus Basin. International Journal of Remote Sensing, 33, 2603 - 2627, 2012.

Cheema, M. J. M., Immerzeel, W. W. and Bastiaanssen, W. G. M.: Spatial Quantification of Groundwater Abstraction in the Irrigated Indus Basin. Ground Water, 52: 25–36. doi: 10.1111/gwat.12027, 2014.

Cuartas, L. A., Tomasella, J., Nobre, A. D., Nobre, C. A., Hodnett, M. G., Waterloo, M. J., de Oliveira, S. M., von Randow, R., Trancoso, R., and Ferreira, M.: Distributed hydrological modeling of a micro-scale rainforest watershed in Amazonia: Model evaluation and

advances in calibration using the new HAND terrain model, Journal of Hydrology, Volumes 462–463, 10 15-27, 2012.

Dahmen, E. R., and Hall, M. J.: Screening of Hydrological Data. Tests for stationarity and Relative Consistency. Publication 49. International Institute for Land Reclamation and Improvement/ILRI, Wageningen, Netherlands, 58 pp, 1990.

De Groen, M. M. and Savenije, H. H. G.: A monthly interception equation based on the statistical characteristics of daily rainfall, Water Resour. Res., 42, 1–10, W12417, doi:10.1029/2006WR005013, 2006.

De Troch, F. P., Troch, P. A., Su, Z., and Lin, D. S.: Application of Remote Sensing for Hydrological Modelling, in Distributed Hydrological Modelling, edited by M. B. Abbott and J. C. Refsgaard, pp. 165-192, Kluwer Academic Publishers, Dordrecht / Boston / London, 1996.

Ehret, U., and Zehe, E.: Series distance - an intuitive metric to quantify hydrograph similarity in terms of occurence, amptitude and timing of hydrological events. Hydrology and Earth System Sciences, 15, 877-896, 2011.

FAO/IIASA/ISRIC/ISS-CAS/JRC: Harmonized World Soil Database (version 1.2). FAO, Rome, Italy and IIASA, Laxenburg, Austria, 2012.

Farr, T., Rosen, P., Caro, E., Crippen, R., Duren, R., Hensley, S., Kobrick, M., Paller, M., Rodriguez, E., Roth, L., Seal, D., Shaffer, S., Shimada, J., Umland, J., Werner, M., Oskin, M., Burbank, D., and Alsdorf, D.: The Shuttle Radar Topography Mission, Rev. Geophysics, 45, RG2004, doi:10.1029/2005RG000183, 2007.

Fu, B., Wang, J., Chen, L., and Qiu, Y.: The effects of land use on soil moisture variation in the Danangou catchment of the Loess Plateau, China. CATENA, 54 (1–2), 197-213, 2003.

Gerrits, A. M. J.: Hydrological modelling of the Zambezi catchment from gravity measurements, Master's thesis, Delft, University of Technology, Delft, The Netherlands, 2005.

Gerrits, A. M. J.: The role of inetrception in the hydrological cycle, PhD thesis, Delft, University of Technology, Delft, The Netherlands, 2010.

Grossmann, M.: Kilimanjaro Aquifer. In: Conceptualizing Cooperation for Africa's Transboundary Aquifer Systems, edited by: Scheumann, W. and Herrfahrdt-Pähle, E., DIE Studies Nr. 32, German Development Institute, 87-125, Bonn, 2008.

Gu, R. R., and Li, Y.: River temperature sensitivity to hydraulic and meteorological parameters. Journal of Environmental Management, 66, 43-56, 2002.

Gupta, H. V., Kling, H., Yilmaz, K. K., and Martinez, G. F.: Decomposition of the mean squared error and nse performance criteria: Implications for improving hydrological modelling, Journal of Hydrology, 377, 80–91, 2009.

Haque, M. F. R.: Validation of TRMM Rainfall data for hydrological applications in Pangani River Basin in Tanzania. MSc Thesis, WSE-HWR-09.05. UNESCO-IHE, 2009.

Hong, Y., Hsu, K. -L., Moradkhani, H., and Sorooshian, S.: Uncertainty quantification of satellite precipitation estimation and Monte Carlo assessment of the error propagation into hydrologic response. Water Resources Research, 42, W08421, doi:08410.01029/02005WR004398, 2006.

Huffman, G. J., Adler, R. F., Morrissey, M. M., Bolvin, D. T., Curtis, S., Joyce, R., McGavock, B., and Susskind, J.: Global precipitation at one-degree daily resolution from multisatellite observations. Journal of Hydrometeorology 2, 36-50, 2001.

Immerzeel, W. M., and Droogers, P.: Calibration of a ditributed hydrological model based on satellite evapotranspiration. Journal of Hydrology, 349, 411-424, 2008.

Karssenberg, D., Burrough, P. A., Sluiter, R., and De Jong, K.: The PcRaster Software and Course Materials for Teaching Numerical Modelling in the Environmental Sciences. Transactions in GIS, 5(2), 99-110, [doi:10.1111/1467-9671.00070], 2001.

Kiptala, J. K., Mohamed, Y., Mul, M., Cheema, M. J. M., and Van der Zaag, P.: Land use and land cover classification using phenological variability from MODIS vegetation in the Upper Pangani River Basin, Eastern Africa. Journal of Physics and Chemistry of the Earth, 66, 112-122, 2013a.

Kiptala, J. K., Mohamed, Y., Mul, M. L and Van der Zaag, P.: Mapping evapotranspiration trends using MODIS images and SEBAL model in a data scarce and heterogeneous landscape in Eastern Africa. Water Resources Research, 49, 1-16, doi: 10.1002/2013WR014240, 2013b.

Komakech, H. C., Van der Zaag, P., and Van Koppen, B.: The last will be first: Water transfers from agriculture to cities in the Pangani river basin, Tanzania. Water Alternatives, 5(3), 700-720, 2012.

Korres, W., Reichenau, T. G., Schneider, K.: Patterns and scaling properties of surface soil moisture in an agricultural landscape: An ecohydrological modeling study. Journal of Hydrology, 498, 89 - 102, 2013.

Kosgei, J. R., Jewitt, G. P. W., Kongo, V. M., and Lorentz, S. A.: The influence of tillage on field scale water fluxes and maize yields in semi-arid environments: A case study of Potshini catchment, South Africa. Physics and Chemistry of the Earth, 32 (15–18), 1117-1126, 2007.

Lenhart, T., Eckhardt, K., Fohrer, N., and Frede, H. -G.: Comparison of two different approaches of sensitivity analysis. Physics and chemistry of the Earth, 22, 645-654, 2002.

Liu, Y. B., and De Smedt, F.: WetSpa Extension. A GIS-Based Hydrologic Model for Flood Prediction and Watershed Management. Documentation and User Manual. Department of Hydrology and Hydraulic Engineering. Vrije Universiteit, Brussel, Belgium, 2004.

Makurira, H., Savenije, H. H. G. and Uhlenbrook, S.: Modelling field scale water partitioning using on-site observations in sub-Saharan rainfed agriculture. Hydrology and Earth System Sciences, 14, 627-638, 2010.

McDonnell, J. J., Sivapalan, M., Vache, K., Dunn, S., Grant, G., Haggerty, R., Hinz, C., Hooper, R., Kirchner, J., Roderick, M. L., Selker, J., and Weiler, M.: Moving beyond heterogeneity and process complexity: A new vision for watershed hydrology, Water Resources Research, 43, W07301, doi:10.1029/2006WR005467, 2007.

Misana, S., Sokoni, C., and Mbonile, M.: Land-use/cover changes and their drivers on the slopes of Mount Kilimanjaro, Tanzania. Journal of Geography and Regional Planning, 5(6), 151-164, 2012.

Mohamed, Y. A., Bastiaanssen, W. G. M., and Savenije, H. H. G.: Spatial variability of evaporation and moisture storage in the swamps of the upper Nile studied by remote sensing techniques. Journal of Hydrology, 289, 145-164, 2004.

Murphy, A. H.: The coefficients of correlation and determination as measures of performance in forecast verification. Weather and forecasting 10(4): 681-688, 1995.

Nash, J. E., Sutcliffe, J. V.: River flow forecasting through conceptual models part I. A discussion of principles. Journal of Hydrology, 10(3), 282-290, 1970.

Nelder, A. J., and Mead, R.: A simplex method for function minimization. Computer Journal, 7, 308-313, 1965.

Nobre, A. D., Cuartas, L. A., Hodnett, M. G., Rennó, C. D., Rodrigues, G., Siveira, A., Waterloo, M. J., Saleska, S.: Height above the nearest drainage – a hydrologically relevant new terrain model. Journal of Hydrology, 404 (1–2), 13–29, 2011.

Norman, J. M., Kustas, W. P., and Humes, K. S.: A two-source approach for estimating soil and vegetation energy fluxes in observations of directional radiometric surface temperature. Agriculture for Meteorology, 77, 263-293, 1995.

Notter, B., Hurni, H., Wiesmann, U., and Abbaspour, K. C.: Modelling water provision as an ecosytem service in a large East African river basin. Hydrology and Earth System Sciences, 16, 69-86, 2012.

PBWO/IUCN: The Hydrology of the Pangani River Basin. Report 1: Pangani River Basin Flow Assessment Initiative, Moshi, 62 pp, 2006.

Prathapar, S. A. and Qureshi, A. S.: Mechanically reclaiming abandoned saline soils: A numerical evaluation, International Water Management Institute, Colombo, Sri Lanka, 1999.

Rijtema, P. E. and Aboukhaled A.: Crop water use, in: Research on crop and water use, salt affected soils and drainage in the Arab Republic of Egypt, edited by: Aboukhaled, A., Arar, A., Balba, A. M. et al., FAO, Near East Regional Office, Cairo, 5–61, 1975.

Roerink, G. J., Su, Z., and Menenti, M.: S-SEBI: A simple remote sensing algorithm to estimate the surface energy balance. Physics and Chemistry of the Earth, Part B - Hydrology, Oceans and Atmosphere, 26, 139-168, 2000.

Romaguera, M., Kros, M. S., Salama, M. S., Hoekstra, A. Y., and Su, Z.: Determining irrigated areas and quantifying blue water use in Europe using remote sensing Meteosat Second Generation (MSG) products and Global Land Data Assimilation System (GLDAS) data. Photogrammetric Engineering and Remote Sensing, 78(8), 861 - 873, 2012.

Ruhoff, A. L., Paz, A. R., Collischonn, W., Aragao, L. E. O. C., Rocha, H. R., and Malhi, Y. S.: A MODIS-Based Energy Balance to Estimate Evapotranspiration for clear-sky days in Brazilian Tropical Savannas. Remote Sensing, 4(3), 703-725, 2012.

Salas, J. D., Ramirez, J. A., Burlando, P., and Pielke Sr, R. A.: Stochastic simulation of precipitation and streamflow processes, Ch. 33, in: T.D. Potter and B.R. Colman (eds) Handbook of Weather, Climate and Water: Atmospheric Chemistry, Hydrology and Societal Impacts, Wiley & Sons, New York, pp 607-640, 2003.

Savenije, H. H. G.: Determination of evaporation from a catchment water balance at a monthly time scale. Hydrology and Earth System Sciences, 1, 93-100, 1997.

Savenije, H. H. G.: Equifinality, a blessing in disguise? Hydrological Processes, 15, 2835-2838, 2001.

Savenije, H.H.G.: The importance of interception and why we should delete the term evapotranspiration from our vocabulary. Hydrological Processes 18, 1507–1511, 2004.

Savenije, H.H.G.: Topography driven conceptual modelling (FLEX-TOPO). HESS opinions. Hydrology and Earth System Sciences, 14, 2681-2692, 2010.

Scipal, K., Scheffler, C., and Wagner, W.: Soil moisture-runoff relation at the catchment scale as observed with coarse resolution microwave remote sensing. Hydrology and Earth System Sciences, 9, 173-183, 2005.

Schultz, G. A.: Hydrological modeling based on remote sensing information, Advances in Space Research, 13(5), 149-166, 1993.

Seyfried, M. S., and Wilcox, B. P.: Scale and the nature of spatial variability: Field examples having implications for hydrologic modeling, Water Resources Research, 31, 173–184, 1995.

Shah, S. H. H., Vervoort, R. W., Suweis, S., Guswa, A. J., Rinaldo, A., and van der Zee, S. E. A. T. M.: Stochastic modelling of salt accumulation in the root zone due to capillary flux from brackish groundwater. Water Resources Research, 47, W09506, doi:10.1029/2010WR009790.

Shrestha, R., Tachikawa, Y., and Takara, K.: Selection of scale for distributed hydrological modelling in ungauged basins. IAHS Publications, 309, 290-297, 2007.

Steduto, P., Hsiao, T. C., Raes, D., and Fereres, E.: AquaCrop – The FAO crop model to simulate yield response to water: I. Concepts and underlying principles, Agronomy Journal, 101, 426–437, 2009.

Su, Z.: The Surface Energy Balance System (SEBS) for estimation of turbulent heat fluxes. Hydrology and Earth Systems Sciences, 6, 85-99, 2002.

Tsiko, C. T., Makurira, H., Gerrits, A. M. J., Savenije, H. H. G.: Measuring forest floor and canopy interception in a savannah ecosystem. Physics and Chemistry of the Earth 47 - 48, 122 - 127, 2012.

Uhlenbrook, S., Roser, S., and Tilch, N.: Hydrological process representation at the meso-scale: the potential of a distributed, conceptual catchment model. Journal of Hydrology, 291, 278–296, 2004.

Wiegand, C. L., Richardson, A. J., Escobar, D. E., Gerberman, A. H.: Vegetation indices in crop assessments. Remote Sensing of Environment 35, 105–119, 1991.

Wilson, E. M.: Engineering Hydrology (3rd Ed.), Macmillan Education Ltd, London, UK, 1983.

Winsemius, H. C., Savenije, H. H. G., and Bastiaanssen, W. G. M.: Constraining model parameters on remotely sensed evaporation: justification for distribution in ungauged basins? Hydrology and Earth System Sciences, 12, 1403-1413, 2008.

Winsemius, H. C., Savenije, H. H. G., Gerrits, A. M. J., Zapreeva, E. A., and Klees, R.: Comparison of two model approaches in the Zambezi river basin with regard to model reliability and identifiability. Hydrology and Earth System Sciences, 10, 339-352, 2006.

Zhang, G. P., Savenije, H. H. G.: Rainfall-runoff modelling in a catchment with a complex groundwater flow system: application of the Representative Elementary Watershed (REW) approach. Hydrology and Earth System Sciences, 9, 243 - 261, 2005.

Zhang, X., Pei, D., and Hu, C.: Conserving groundwater for irrigation in the North China Plain. Irrigation Sciences, 21, 159–166, 2003.

Table 1. Model performance for the modified STREAM model for Upper Pangani River Basin.

Station	Calibration				Validation			
	E	E_{ln}	MAE (m^3 s^{-1})	RMSE (m^3 s^{-1})	E_{ns}	E_{ns_ln}	MAE (m^3 s^{-1})	RMSE (m^3 s^{-1})
1dc8a	0.63	0.68	0.73	0.92	0.72	0.68	0.62	0.36
1d5b	0.75	0.77	0.74	1.09	0.81	0.78	0.57	0.23
1dd11a	0.46	0.64	0.84	1.14	0.33	0.69	0.94	0.88
1dd54	0.70	0.60	2.31	8.06	0.42	0.61	1.99	5.84
1dd1	0.84	0.90	2.08	9.34	0.83	0.90	1.74	4.78

Table 2. Sensitivity of model performance due to change in model input parameters.

Parameter	Input Values			Resulted RMSE ($m^3 s^{-1}$)					Resulted MAE ($m^3 s^{-1}$)				
	x_1	x_0	x_2	y_1	y_0	y_2	SI (x_1)	SI (x_2)	y_1	y_0	y_2	SI (x_1)	SI (x_2)
D [mm day^{-1}]	0	2.5	4	8.8	6.9	7.1	-0.12	0.02	2.0	1.8	1.8	-0.12	0.01
$S_{u, Max}$ [mm]	262	350	438	12.4	6.9	6.9	**-1.97**	0.04	2.1	1.8	1.8	-0.47	0.19
$S_{s, Max}$ [mm]	150	200	250	9.3	6.9	8.0	**-1.00**	0.48	2.2	1.8	2.2	-0.64	0.66
c_r [-]	0	0.75	1.0	202.5	6.9	16.6	**-0.93**	**1.25**	9.6	1.8	2.9	-0.69	0.71
q_c [-]	0	0.75	1.0	39.7	6.9	7.7	-0.70	0.20	5.4	1.8	1.9	-0.50	0.07
C_{max} [mm day^{-1}]	1.5	2.0	2.5	7.2	6.9	7.1	-0.14	0.08	2.0	1.8	1.8	-0.34	0.00
f [-]	0.25	0.33	0.41	6.9	6.9	7.1	0.00	0.07	1.8	1.8	1.8	0.00	0.10
K_o [8-day]	-	1	2	-	6.9	6.9	-	0.00	-	1.8	1.8	-	0.02
K_q [8-day]	1	2	3	7.0	6.9	7.0	0.00	0.02	1.8	1.8	1.9	-0.07	0.08
K_s [8-day]	20	28	35	7.4	6.9	7.5	-0.19	0.27	2.2	1.8	2.0	-0.49	0.27

Table 3. Impact of three water management scenarios on the surface runoff.

Scenario		Action	Impact on outflow (Mm^3 yr^{-1})		
			Total	Base flow	Overland flow
1	Reduce E_s	Reduce E_s for supplementary irrigation (mixed crops) by 15% or approximately 5% of transpiration	37.8	34.5	3.2
2 a	Increase T	Increase T by 30% for rainfed maize in the highlands areas	-84.2	-77.6	-6.6
b		plus 30% increase in $S_{u,max}$	-87.0	-76.9	-10.1
3	Modify area	Double sugarcane irrigated area (additional 7,400ha)	-53.9	-53.3	-0.6

LIST OF FIGURES CAPTIONS

Fig. 1. Overview of entire Pangani River Basin and the Upper Pangani River Basin

Fig. 2. Modified STREAM conceptual model for Upper Pangani River Basin.

Fig. 3. Soil moisture depletion fraction (defined using average values of the dry month of January of 2008, 2009 and 2010) in the Upper Pangani River Basin for selected land use types.

Fig. 4. (a) Wetland - Hillslope (Snowmelt) hydrological system **(b)** Shallow groundwater observation wells with mean surface water levels (0.3 - 40 m) in the lower catchments of the Upper Pangani River Basin for the period 2008-2010.

Fig. 5 (1 - 4). (a) Comparison of observed (Qo) and the simulated discharge (Qs) and precipitation at the outlet points for calibration period 2008 (8-day periods 1 - 46) and validation 2009, 2010 (8-day periods 47 - 138) in the Upper Pangani River Basin; and **(b)** the corresponding scatter plots of Qo and Qs for four upstream gauge stations

Fig. 6. (a) Comparison of observed (Qo) and simulated discharge (Qs) and precipitation for calibration period 2008 (8 day periods 1–46) and validation 2009, 2010 (8 day periods 47–138) in the Upper Pangani River Basin; and **(b)** the corresponding scatter plot of Qo and Qs for the most downstream gauge station.

Fig. 7. Mean Interception, I, and evaporation depletion, $E + T$ for different land use classes in Upper Pangani River basin for Period 2008 - 2010.

Fig. 8. Spatial Variability of **(a)** land use map (Kiptala et al., 2013a) **(b)** ET_a averaged for 2008-2010 (Kiptala et al., 2013b) and **(c)** Blue water use (Q_b) averaged over 2008 - 2010 in the Upper Pangani River Basin.

Fig. 9. ET_a and the corresponding Q_g and Q_b water use for selected land use types averaged per year over 2008 - 2010 in the Upper Pangani River Basin (Error bar indicates the upper and lower bounds for mean Q_b for dry year 2009 and wet year 2008 respectively).

Fig. 10. Total net irrigation water use ($Q_{b(I)}$) estimated upstream of the gauge stations using modified STREAM model in the Upper Pangani River Basin (averaged over years 2008-2010).
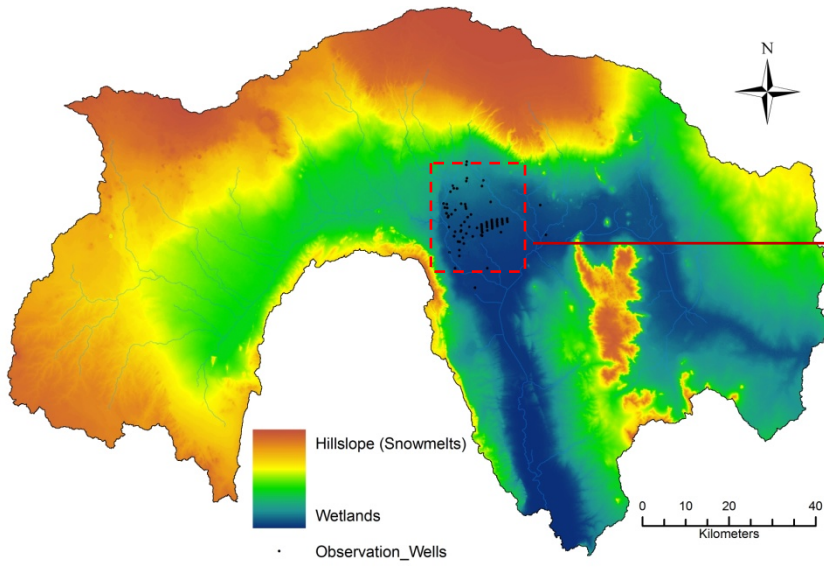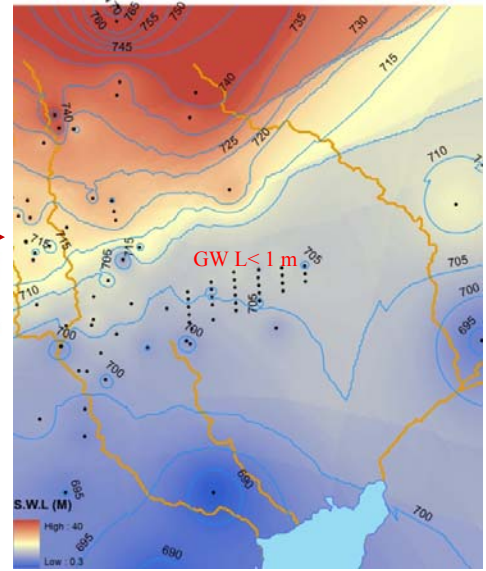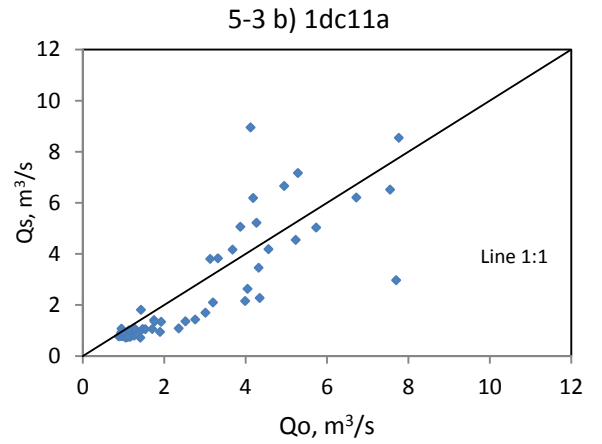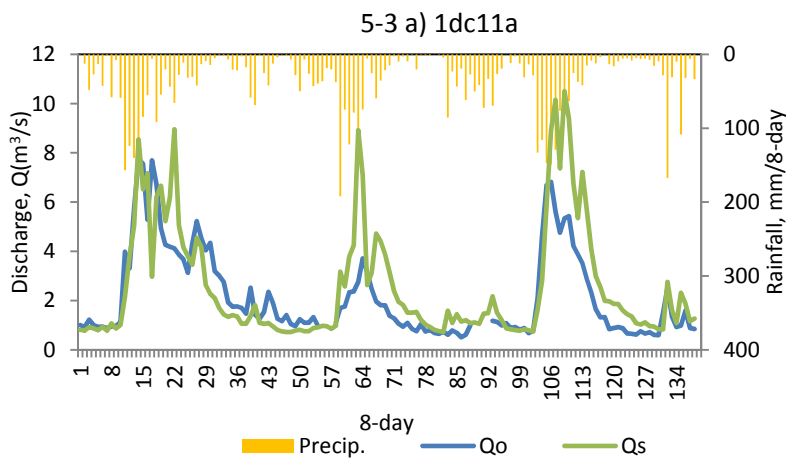
30

P(t) I(t) $P_e(t)$

D

$c_r.P_e(t)$ E +T (t) $(1-c_r)P_e(t)$

Q_u

$S_{u,max}$
S_u
$S_{u,min}$

$Q_b(t)$

Additional
Bucket

S_b

S_s

K_o
$S_{S,max}$ $Q_o(t)$

K_q $Q_q(t)$
$S_{S,q}$

C(t) $S_{c,min}$

K_s $Q_{s,g}(t)$
$S_{s,min}$

$Q_{s1}(t)$

-$Q_d(t)$

$Q_s(t)$
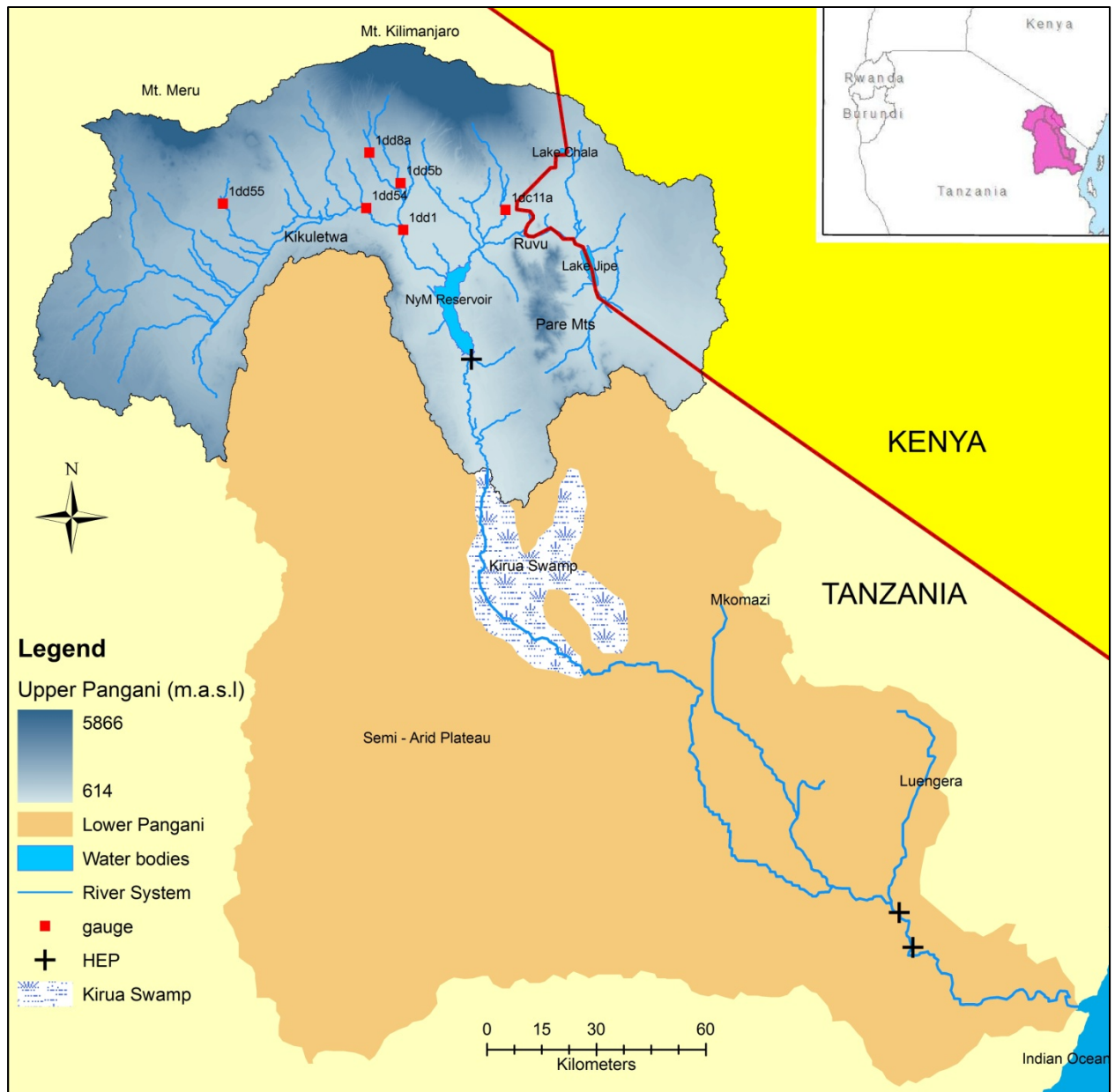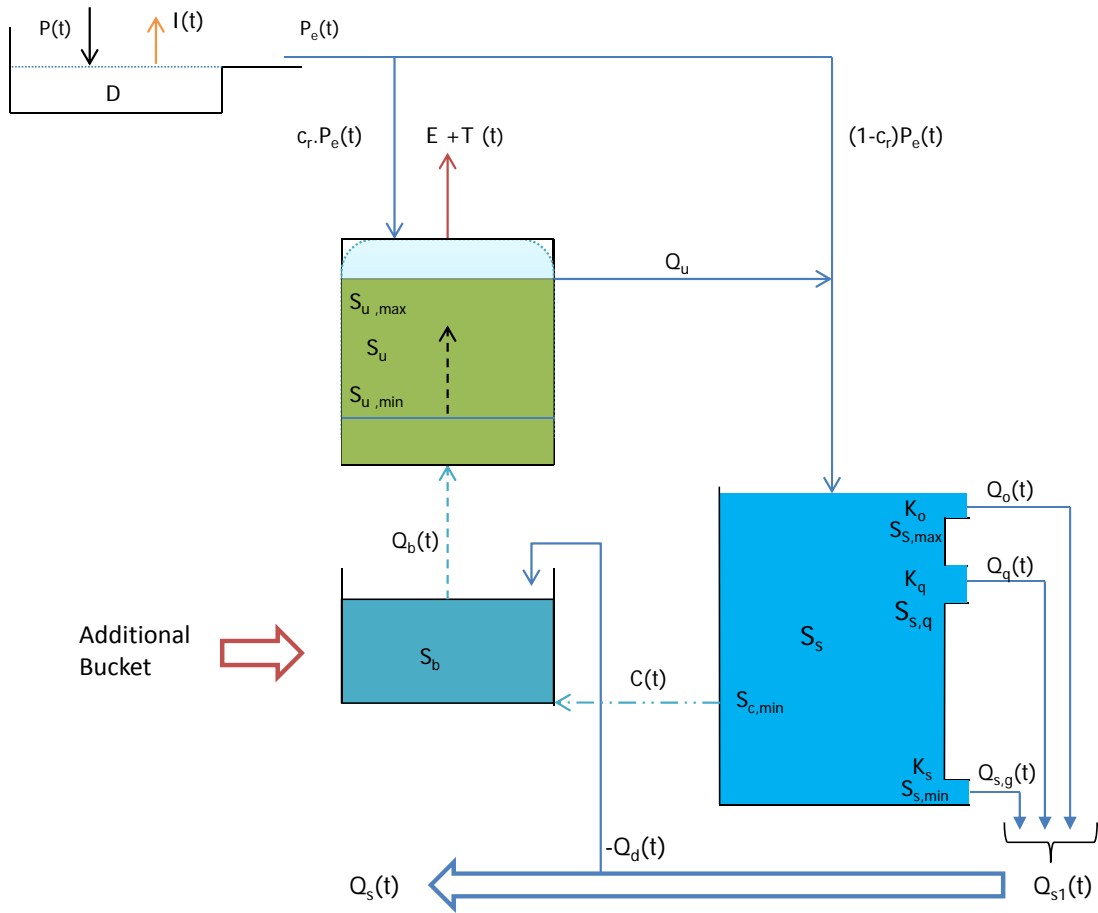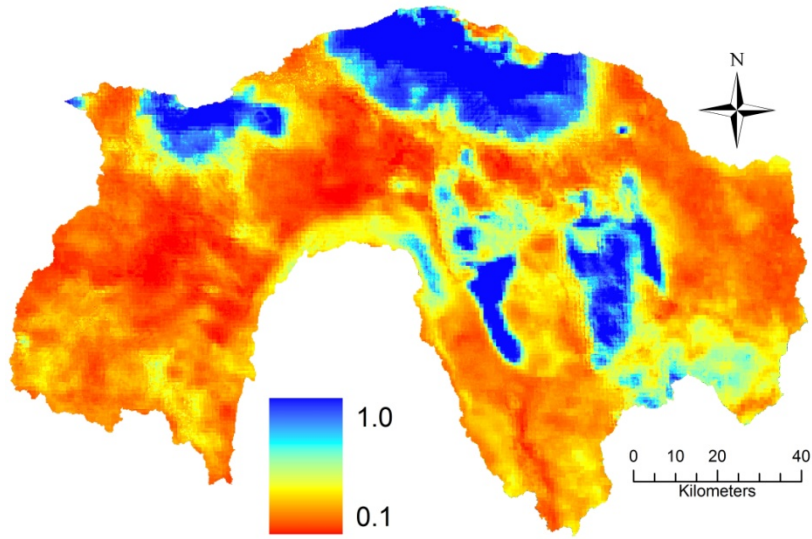
Land Use Type	Depletion fraction (f)
Water Bodies	0.87
Sparse Vegetation	0.27
Bushlands	0.29
Rainfed, Maize	0.30
Irrigation, Sugarcane	0.46
Irrigation; Bananas, coffee Mixed crops	0.60
Dense Forest	0.72

a)

Hillslope (Snowmelts)

Wetlands

· Observation_Wells

0 10 20 40
Kilometers

N

b)

GW L< 1 m

S.W.L (M)

High : 40

Low : 0.3

41

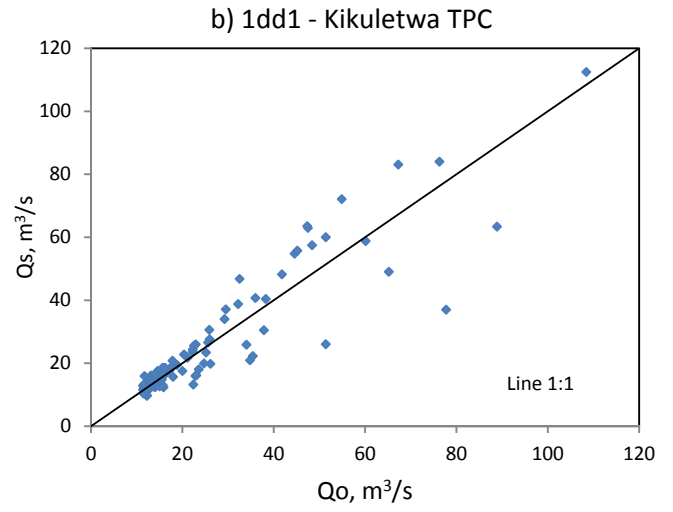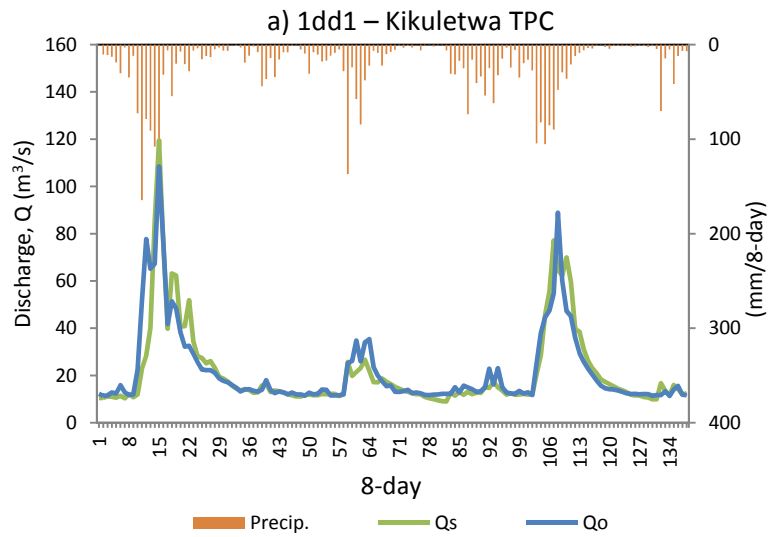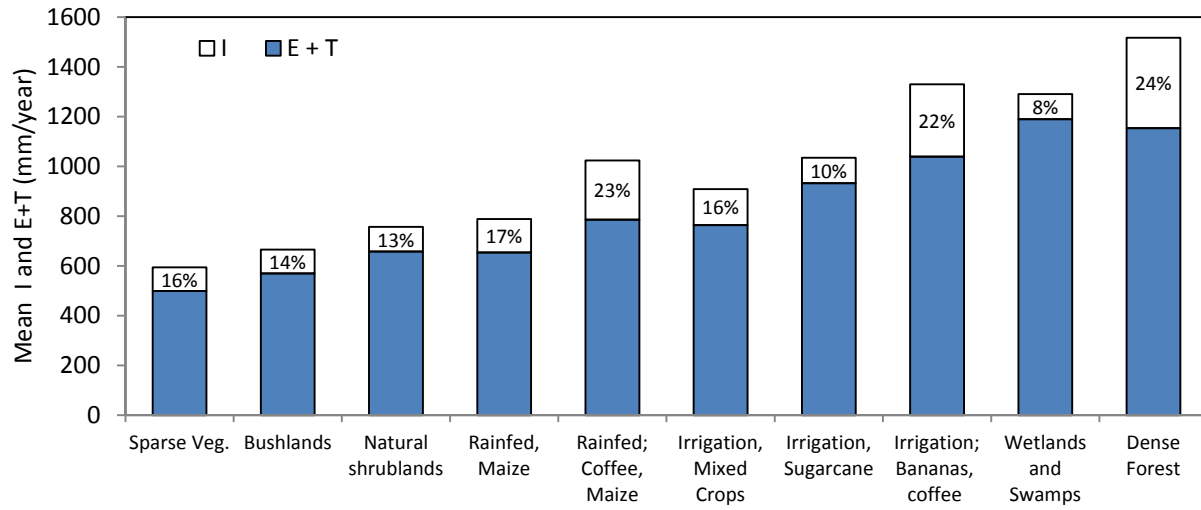5-1 a) 1dc8a

5-1 b) 1dc8a

5-2 a) 1dc5b

5-2 b) 1dc5b

5-3 a) 1dc11a

5-3 b) 1dc11a

5-4 a) 1dd54

5-4 b) 1dd54

a) 1dd1 – Kikuletwa TPC

b) 1dd1 - Kikuletwa TPC

Line 1:1

a)

Class

■ Water bodies	■ Grasslands, scattered croplands	■ Irrigated mixed crops	■ Irrigated bananas and coffee
■ Bareland	■ Shrublands and thicket	■ Rainfed maize, coffee	■ Dense forest
■ Sparse vegetation	■ Rainfed maize	■ Irrigated sugarcane	■ Wetlands and swamp
■ Bushlands	■ Afro-Alpine forest	■ Forest and croplands	■ Urban and built-up areas

b)

ETa [mm/yr]

2223

0

5

c)

Qb [mm/yr]

1642

0

46

Qb(I) (m3/s)

- 0.06 - 1dd8a/5b
- 0.17 - 1dd55
- 0.19 - 1dd11a
- 1.95 - 1dc2a
- 2.01 - 1dd54
- 2.77 - 1dd1
- 3.38 - 1dc
- 4.20 - 1dd